Information-theoretic analysis of a stimulated-Brillouin-scattering-based slow-light system

Myungjun Lee,[1,*] Yunhui Zhu,[2] Daniel J. Gauthier,[2] Michael E. Gehm,[1] and Mark A. Neifeld[1]

[1]Department of Electrical Computer Engineering and College of Optical Sciences, University of Arizona, Tucson, Arizona, 85721-0104, USA

[2]Department of Physics and the Fitzpatrick Institute for Photonics Duke University, Durham, North Carolina, 27708 USA

*Corresponding author: mjlee76@email.arizona.edu

Received 10 August 2011; accepted 12 September 2011; posted 19 September 2011 (Doc. ID 152507); published 3 November 2011

We use an information-theoretic method developed by Neifeld and Lee [J. Opt. Soc. Am. A **25**, C31 (2008)] to analyze the performance of a slow-light system. Slow-light is realized in this system via stimulated Brillouin scattering in a 2 km-long, room-temperature, highly nonlinear fiber pumped by a laser whose spectrum is tailored and broadened to 5 GHz. We compute the information throughput (IT), which quantifies the fraction of information transferred from the source to the receiver and the information delay (ID), which quantifies the delay of a data stream at which the information transfer is largest, for a range of experimental parameters. We also measure the eye-opening (EO) and signal-to-noise ratio (SNR) of the transmitted data stream and find that they scale in a similar fashion to the information-theoretic method. Our experimental findings are compared to a model of the slow-light system that accounts for all pertinent noise sources in the system as well as data-pulse distortion due to the filtering effect of the SBS process. The agreement between our observations and the predictions of our model is very good. Furthermore, we compare measurements of the IT for an optimal flattop gain profile and for a Gaussian-shaped gain profile. For a given pump-beam power, we find that the optimal profile gives a 36% larger ID and somewhat higher IT compared to the Gaussian profile. Specifically, the optimal (Gaussian) profile produces a fractional slow-light ID of 0.94 (0.69) and an IT of 0.86 (0.86) at a pump-beam power of 450 mW and a data rate of 2.5 Gbps. Thus, the optimal profile better utilizes the available pump-beam power, which is often a valuable resource in a system design.

OCIS codes: 200.3050, 060.4510, 290.5900, 260.2030, 060.4370, 190.2640.

1. Introduction

In recent years, slow and fast light techniques that enable dynamic control of the group refractive index of light traveling through dispersive devices have received a great deal of attention [1]. Continuously tunable delay lines are of interest in optical telecommunication for data buffering, synchronization, and jitter correction [2,3], for example, as well as in interferometry for scanning a reference arm without moving parts [4–6] and slow-light laser radar [7]. As a result, achieving slow-light in a wide variety of material systems using different physical mechanisms have been under intensive study, including the popular realization of slow-light using stimulated Brillouin scattering (SBS) [8–10], which is the focus of this paper. Substantial progress has been made toward improving the maximum achievable fractional delay (i.e., equivalent to the delay–bandwidth product) of SBS slow-light while simultaneously minimizing signal distortion by tailoring the resonance profile [11–26]. Nonetheless, due to the inevitable higher-order material dispersion and spectral filtering effects, the pulse shape always suffers at least

0003-6935/11/326063-10$15.00/0

some distortion that limits the slow-light device performance for many applications.

There exist a wide variety of metrics to quantify signal fidelity in a slow-light system, which often are constrained to account for practical considerations such as a required minimum signal-to-noise ratio (SNR) of the received delayed signal, the size of the device, or a limit to the power used to induce the slow-light effect [2]. Each of these approaches lead to different system parameters that optimize the slow-light effect for a particular application. For telecommunication applications, where a random stream of closely-spaced pulses propagate through the channel, generalized pulse distortion can lead to a bleed-over of energy from 1 bit slot to its neighbors (intersymbol interference), thereby degrading the receiver's ability to unambiguously determine the transmitted bit sequence. Several notable studies of delay–bandwidth and storage capacity bounds have been undertaken for linear optical devices that focus on the pulse broadening factor, eye-opening (EO), bit error rate, and SNR [2,27–29].

Recently, Neifeld and Lee [30] developed an alternative method for analyzing slow-light delay devices using an information-theoretic framework. In particular, their approach uses the Shannon mutual information [31] to quantify the information contained in a measured signal arising from a finite-duration data sequence for a specific choice of an input-output signaling protocol. This analysis method can be used to determine the time at which the largest fraction of the input information is available at the output receiver, as quantified through the information delay (ID) and information throughput (IT). Relatedly, both the ID and IT can be used in an optimization strategy to improve the performance of the slow-light device.

The primary purpose of this paper is to apply the information-theoretic analysis method [30] to a broadband SBS-based slow-light system in the presence of distortion and noise and use it to optimize its performance. In the next section, we give an overview of the slow-light system. In Section 3, we review the IT analysis method and compare it to more traditional EO- and SNR-based metrics. In Section 4, we develop a theoretical model for the slow-light system, including noise sources. Using these metrics, we explore in Section 5 how the slow-light system performance depends upon the various parameters such as pump powers, input probe powers, data rate, and shape of the gain profile. Section 6 pulls together our findings in a discussion and conclusion.

2. Slow-Light System Overview

Before summarizing our analysis methods, we give a brief overview of the slow-light system. The broadband SBS-based slow-light system is shown schematically in Fig. 1(a). A pump-beam (wavelength 1550 nm, power P_p) is generated by a distributed feedback laser (DFB) whose injection current is modulated by an arbitrary waveform generator. This beam is amplified by an erbium-doped fiber amplifier and enters the slow-light medium: a 2 km long highly nonlinear fiber (HNLF). A signal beam generated by a second DFB (power $P_{s,\mathrm{in}}$) is modulated by a Mach–Zehnder modulator, which is driven by a pattern generator and counterpropagates through the HNLF with the use of a circulator. To highlight the effects of all sources of noise and signal distortions, we choose values of $P_{s,\mathrm{in}}$ about a nominal "standard" value $P_{\mathrm{in}} = 24\,\mu$W. A fiber polarization controller is used to maximize the transmitted power and a fiber Bragg grating is used as a bandpass filter to remove Rayleigh backscattering induced by the pump-beam. The transmitted probe beam (power $P_{s,\mathrm{out}}$) is directed to a photodiode (responsivity R) using a circulator. A variable optical attenuator in front of the photodiode is set to 7 dB to ensure that the delayed and amplified signal beam are just below the saturation intensity of the photodiode when $P_p = 500$ mW. For $P_{s,\mathrm{in}} = P_{\mathrm{in}}$, saturation of the SBS gain only becomes apparent at $P_p = 400$ mW. The photodiode output voltage is recorded with a 8 GHz bandwidth, 40 Gs/s real-time digital sampling oscilloscope.

To characterize the fidelity of the slow-light system appropriate for an optical communication, we consider the propagation from source to receiver of all 256 possible 8 bit binary sequences, ranging from $[0\ 0\ 0\ 0\ 0\ 0\ 0\ 0]$ to $[1\ 1\ 1\ 1\ 1\ 1\ 1\ 1]$ using a return-to-zero (RZ) format with a 2 bit long buffer of 0s between each sequence. The received signal from each sequence is overlayed based on the trigger generated by the pattern generator. Figure 1(b) shows a portion of the overlayed sequences where the variation in the pulse shapes is due to the pattern dependence of the slow-light effect as well as the various noise sources (described in greater detail in Section 4). Fluctuations in the baseline (the "0" state, mean value u_0) and pulse peaks (the "1" state, mean value u_1) are characterized by the deviations σ_0 and σ_1, respectively, evaluated at the maximum EO of the pattern. These quantities are used to evaluate the fidelity metrics and are compared to our model of the slow-light system.

Clearly, we have chosen specific experimental components and parameters in our study that balance various trade-offs. For example, we are limited by detector noise together with signal distortion and, on the other hand, by saturation of the SBS gain. We also select rectangular pulse shape and use the RZ modulation format for the signal, which are commonly used in slow-light communications applications. Note that, under the given SBS gain spectrum, the choice of different pulse shapes and modulation formats [32] might impact the results. However, our comparison and optimization of system parameters is consistent and the observed trends should be obeyed in all systems. Thus, our study provides useful guidelines for other systems that use different components or slow-light methods.

3. Slow-Light Data Fidelity Metrics

We first summarize two data fidelity metrics that are commonly used by the optical telecommunication and slow-light research communities. The maximum EO represents the difference between the maximum value of the 0s and the minimum value of 1s [see Fig. 1(b)] over all symbol sequences. The time-instance of the maximum EO defines the optimal sampling/decision time for such a receiver. The experimentally measured SNR at the eye-center is given by [33]

$$\mathrm{SNR}_{\mathrm{exp}} = \frac{u_1 - u_0}{\sqrt{\sigma_1^2 + \sigma_0^2}}. \tag{1}$$

The SNR of the system is closely related to other metrics such as EO, bit error rate (BER), and Q factor at the optimal decision level, where $Q = (u_1 - u_0)/(\sigma_1 + \sigma_0)$ and $\mathrm{BER} = \mathrm{erfc}(Q/\sqrt{2})$ [33,34]. The slow-light delay can be determined by using the time difference between the maximum EO (or SNR) instants of the input and output eye diagrams.

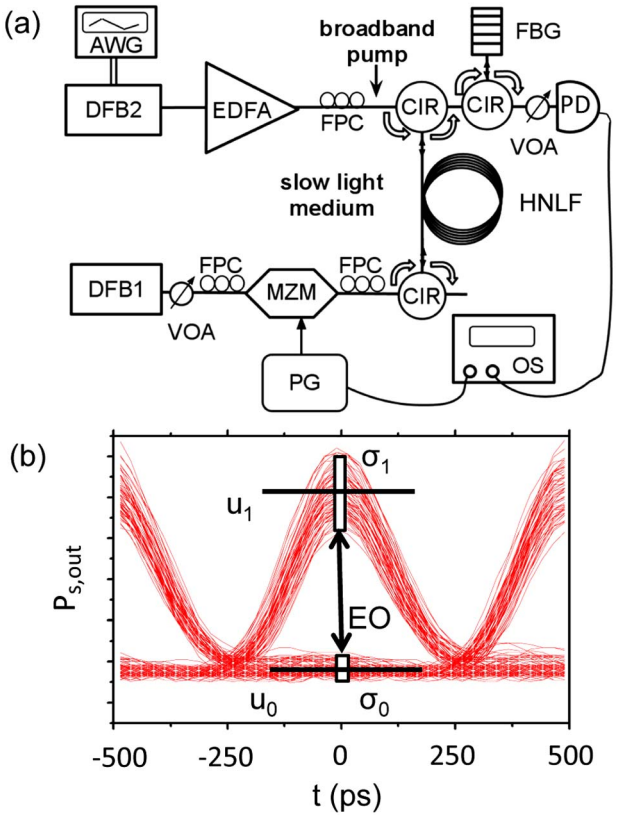

Fig. 1. (Color online) (a) Experiment setup. HNLF: slow-light medium (HNLF, OFS, Inc.) FPC: fiber polarization controller, EDFA: erbium-doped fiber amplifier, CIR: circulator, MZM: Mach–Zehnder modulator, PD: photodiode, FBG: fiber Bragg grating, AWG: arbitrary waveform generator (Tektronix AFG3251), DFB: distributed feedback laser, VOA: variable optical attenuator, OS: oscilloscope and PG: pattern generator (Agilent 70843B). (b) Example of eye diagram measured by an oscilloscope. The vertical box indicates the region of the eye diagram used to measure the standard deviation of "1's" and "0's" at the eye-center.

Recently, Neifeld and Lee [30] introduced an information-theoretic metric that uses Shannon information theory [31] to estimate the IT and ID of a slow-light system. In this approach, the mutual information (MI) is used to determine the information transfer rate between the slow-light input X and output Y, where the MI is defined as $I(X;Y) = H(X) - H(X|Y)$, $H(X)$ denotes the entropy of the binary-valued discrete input X [35], and $H(X|Y)$ is the conditional entropy given the output Y. We assume that the output Y is corrupted by additive white Gaussian noise with zero mean and variance σ^2. In addition, a specific m-bit input sequence $X = [x_1, x_2, \ldots, x_m]$ is assumed to have elements x_i that are independent and identically distributed. The prior probability for any such sequence is $p(x_i) = (1/2)^m$. With these assumptions, we can formally rewrite the MI as

$$I(X;Y) = m + \int \sum_{i=1}^{M} p(x_i)p(Y|x_i)\log_2 \frac{p(x_i)p(Y|x_i)}{\sum_{i=1}^{M} p(x_j)p(Y|x_j)}\mathrm{d}Y, \tag{2}$$

where m is the number of input bits, $M = 2^m$ is the number of possible m-bit input sequences. The probability density function of Y conditioned on x_i is given by

$$p(Y|x_i) \simeq \frac{1}{(2\pi\sigma^2)^{mN}} \exp\left(-\frac{1}{2\sigma^2}|Y - x_i|^2\right), \tag{3}$$

where N is the number of temporal measurements in a bit slot.

The slow-light delay cannot be determined simply using the definition of the MI (Eq. (2)). This issue can be addressed using a temporal window that contains the input pulse sequence [30]. In this way, one can compute the MI between the input X and only that part of Y contained in the finite output window as a function of the output window offset. The maximum value of the MI as a function of the offset t_{off} then defines the normalized IT as $\mathrm{IT} = \max_{t_{\mathrm{off}}}\{I(X;Y)\}/m$ and the location of this maximum defines the ID of the delay device. Figure 2 is a schematic illustration of this approach for an ideal distortion- and noise-free delay device ($\sigma = 0$). For the sake of illustration, we use a 3 bit sequence ($m = 3$) consisting of RZ Gaussian pulses with bit period of 100 ps as an input to the delay channel, which has a delay of 400 ps. When the window offset is the same as the system delay (400 ps), a MI of 3 bits is obtained because all the input signal information can be transferred to the output without any loss due to distortion, noise or energy leakage outside the window.

The integral over Y in Eq. (3) is evaluated for the experimental data using the following procedure. The first step is to generate an approximation to a noiseless data stream representing each bit pattern.

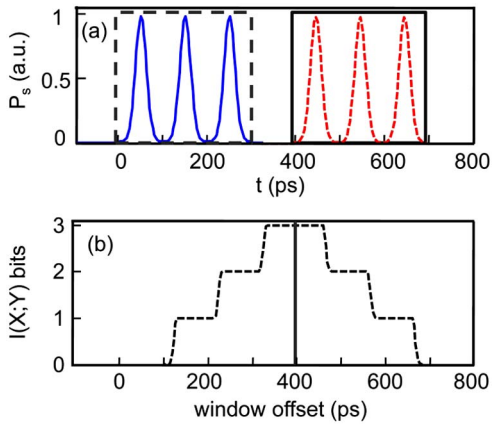

Fig. 2. (Color online) Application of the IT analysis to an ideal delay device. (a) Example signals at the output of the slow-light medium in the absence (solid blue line) and presence (dashed red line) of the slow-light effect. (b) Mutual information as a function of output window. The vertical dashed line indicates the middle of the region of high mutual information, which determines the information delay.

We estimate the noiseless waveforms by turning off the pump-beam ($P_p = 0$), pass all possible 8 bit sequences through the system 100 times, and average the resulting waveforms. We then fit to the averaged data a sequence of numerically-generated noise-free waveforms consisting of RZ super-Gaussian pulses corresponding to each bit pattern; these theoretical waveforms are then taken as the noise-free input bit patterns. The next step is to turn on the pump-beam and pass all possible 8 bit sequences through the system 100 times. By comparison with the ideal sequences, it is possible to estimate σ^2 and $p(Y|x_i)$. Finally, $I(X;Y)$ is determined using a Monte Carlo technique to evaluate the integral. In the theoretical model, we have access to the noise-free waveform; the integral is evaluated for 100 noise realizations.

4. System Modeling

In this section, we summarize the theoretical model for the SBS interaction, which is extended beyond typical textbook results to account for broadening of the resonance via spectral broadening of the pump field. We also develop models for the various noise sources in the system.

A. Stimulated Brillouin Scattering

The geometry of the SBS interaction is shown in Fig. 3. The SBS process results from the nonlinear mixing between a strong pump wave (electric field

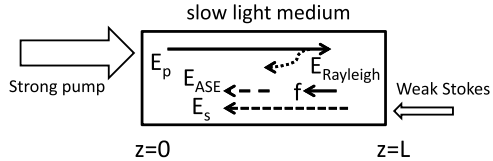

Fig. 3. Geometry of the SBS interaction. Complex field amplitudes for the signal, pump and Rayleigh back scattered waves, are denoted by E_s, E_p, and E_{Rayleigh}, respectively, and the Langevin noise source is denoted by f.

amplitude $E_p(z,t)$, frequency ω_p) traveling in the z-direction, a weak counterpropagating Stokes wave (amplitude $E_s(z,t)$, frequency ω_s), and an acoustic wave induced by the optical waves via electrostriction. The Stokes wave experiences amplification due to its mutual interaction between the pump and acoustic waves. Large amplification is possible when $(\omega_p - \omega_s) - \Omega_B < \Gamma_B$, where Ω_B (Γ_B) denotes the Brillouin frequency shift (resonance linewidth). For slow-light buffer applications, the data sequence is encoded on the Stokes wave.

For typical silica single-mode fibers, $\Gamma_B/2\pi \sim$ 30 MHz, which limits the usable data rate to only several tens of Mbits/s. Several methods have been developed for broadening the SBS resonance linewidth to the gigahertz range, making it relevant for current optical telecommunication systems. It is also possible to simultaneously tailor the shape of the broadened resonance to minimize pulse distortion [11–26]. It has been shown that a flattop SBS gain profile minimizes distortion and increases the slow-light delay [19–21,26]. In our experiments described below, we generate a nearly ideal flattop SBS gain profile with a spectral width (full-width at half-maximum) $\Delta\Omega_G/2\pi = 5$ GHz by broadening the spectrum of the pump laser (see Fig. 1) using a tailored noisy injection current described in detail in [26].

In our theoretical analysis, we assume for simplicity that the signal wave is so weak that it does not deplete the pump wave. In this case, the evolution of the Stokes wave in the spectral domain is governed by the transfer function of the slow-light channel [10,11,16,19,36]. For an ideal rectangular-shaped, flattop SBS gain profile, the power spectral density (PSD) of the signal wave is given by

$$\tilde{P}_s(0,\Delta\omega) = \tilde{P}_s(L,\Delta\omega)H_{\text{SBS}}, \tag{4}$$

where the SBS transfer function is given by

$$H_{\text{SBS}} = \exp(-\alpha L)\exp[G_B B(\Delta\omega)L_{\text{eff}}]. \tag{5}$$

Here, $\tilde{P}_s(L,\Delta\omega)$ is the input signal PSD, $\Delta\omega = \omega - \omega_p + \Omega_B$, α is the material intensity absorption coefficient, L is the fiber length, $G_B = g_0\pi I_p\Gamma_B/2\Delta\omega_G$ is the SBS gain factor, g_0 is the SBS gain coefficient, I_p is the pump intensity at $z = 0$, $L_{\text{eff}} = 1 - \exp(-\alpha L)/\alpha$ is the effective fiber length, and

$$B(\Delta\omega) = \frac{1}{\pi}\left[\tan^{-1}\left(\frac{\Delta\omega + \Delta\omega_G/2}{\Gamma_B/2}\right) - \tan^{-1}\left(\frac{\Delta\omega - \Delta\omega_G/2}{\Gamma_B/2}\right)\right] \tag{6}$$

is the lineshape function. When $\Delta\omega_g \gg \Gamma_B$ as in our experiment, the full-width at half-maximum of the gain lineshape is equal to $\Delta\omega_g$. Equations (4) and (6) show that the signal experiences exponential gain with an exponential gain coefficient that is

proportional to the pump intensity and material length and inversely proportional to the spectral bandwidth of the resonance when its frequency is in the vicinity of the Stokes resonance. Using the Kramers–Kronig relation, it is possible to show that the slow-light delay is related to this exponential gain coefficient [37].

For situations where the spectrum of the data-encoded input signal wave extends beyond the bandwidth of the SBS gain resonance, spectral filtering occurs, causing pattern dependence of the transmitted data sequence. Pattern dependence causes power to spill over into neighboring bit slots and hence causes signal-amplitude variation. To account for the pattern dependence in our theoretical simulations, we determine numerically the amplitude jitter at the maximum EO for all 256 data patterns encoded on the Stokes wave after propagation through the slow-light channel. We assume, for simplicity, that the amplitude jitter is described by a Gaussian distribution with variance σ_{j1} and the mean amplitude of a "1" is equal to u_{j1}. The amplitude jitter causes a mean-square current fluctuation at the detector output equal to [33,34,38,39]

$$\sigma_{\mathrm{aj}}^2 = R^2(P_{s,\mathrm{out}}\sigma_{j1}/u_{j1})^2, \tag{7}$$

where $P_{s,\mathrm{out}} = \int \tilde{P}_s(0,\Delta\omega)\mathrm{d}\omega$.

B. Amplified Spontaneous Brillouin Scattering

The pump wave also generates scattered light in the absence of a coherent signal due to amplified spontaneous Brillouin scattering, thus degrading the SNR and IT. This noisy wave counterpropagates with respect to the pump wave and has a similar spectral content as the input data stream and hence cannot be removed. Spontaneous Brillouin scattering arises from thermal fluctuations in the fiber, which is subsequently amplified by the SBS process. The pump wave also induces Rayleigh back scattering that copropagates with the signal, as illustrated in Fig. 3. However, Rayleigh scattering has an identical spectrum of the pump wave spectrum and hence can be removed with a narrowband spectral filter that is centered at ω_s, as is done in the experiments. We therefore ignore this potential noise source.

Following Boyd *et al.* [40], we account for amplified spontaneous Brillouin scattering by assuming that the spontaneous scattering is a Langevin process described by a δ-correlated Gaussian random variable with zero mean and correlation amplitude $Q_{\mathrm{th}} = (2k_BT\rho_0\Gamma_B)/(v^2A)$, where k_B is Boltzmann's constant, T is the temperature, ρ_0 is the average material density, v is the speed of sound in the fiber, and A is the effective cross-sectional area of the beams in the fiber [36,40]. The PSD for amplified spontaneous emission (ASE) is then given by

$$\tilde{P}_{\mathrm{ase}}(0,\Delta\omega) = K_{\mathrm{ASE}}\left[H_{\mathrm{SBS}}\left(\exp(-\alpha L) + \frac{\alpha}{G_BB(\Delta\omega)}\right) - \left(1 + \frac{\alpha}{G_BB(\Delta\omega)}\right)\right], \tag{8}$$

with $K_{\mathrm{ASE}} = 2\pi k_BTc/n\Omega_B$. The total PSD for light emitted from the fiber along the signal path is $\tilde{P}_{\mathrm{tot}}(0,\Delta\omega) = \tilde{P}_s(0,\Delta\omega) + \tilde{P}_{\mathrm{ase}}(0,\Delta\omega)$ [41].

The ASE noise power is denoted by $P_{\mathrm{ase}}(0)$ and is approximately equal to $P_{\mathrm{ase}}(0,\Delta\omega=0)\Delta\nu_e$ for a flattop gain profile, where $\Delta\nu_e$ is the effective electrical bandwidth of the receiver. This noisy optical field gives rise to current fluctuations in the detector due to two effects. One is due to the beating of the signal wave with the ASE wave, giving rise to mean-square current fluctuations equal to [33,42]

$$\sigma_{s-sp}^2 = 4R^2P_{s,\mathrm{out}}P_{\mathrm{ase}}(0,\Delta\omega=0)\Delta\nu_e. \tag{9}$$

The other source is due to beating of the noisy ASE wave with itself, giving rise to mean-square current fluctuations equal to

$$\sigma_{sp-sp}^2 = 4R^2P_{\mathrm{ase}}(0,\Delta\omega=0)^2\Delta\nu_e\Delta\nu_o, \tag{10}$$

where $\Delta\nu_o$ is the effective optical bandwidth [33].

Figure 4 illustrates a numerical simulation of the PSD at the input and output of a SBS-based slow-light medium for a flattop gain profile and material parameters appropriate for the HNLF used in the experiments. We use an input signal bit rate (BR) of 2 Gbps with a 50% RZ modulation format, where a single pulse (a "1") occupies half of the bit slot. Thus, the bandwidth of such a data sequence has a bandwidth that is twice as large as the data rate (4 GHz in this example). To ensure the validity of the undepleted-pump approximation, we use $P_{s,\mathrm{in}} = P_{\mathrm{in}}$. As seen in Fig. 4, we predict an exponential gain of five near the center of the spectrum for $P_p = 300$ mW. It is

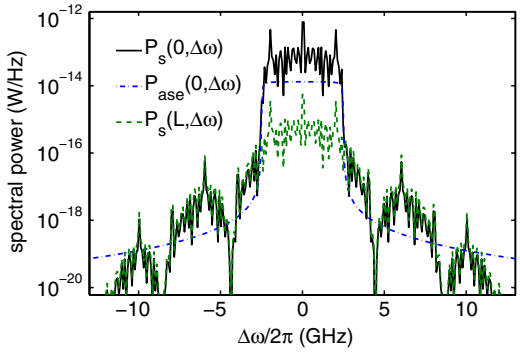

Fig. 4. (Color online) Theoretically predicted power spectral density for the input signal $\tilde{P}_s(L,\Delta\omega)$, amplified signal $\tilde{P}_s(0,\Delta\omega)$, ASE signal $\tilde{P}_{\mathrm{ase}}(0,\Delta\omega)$, and total signal $\tilde{P}_{\mathrm{tot}}(0,\Delta\omega)$ for the case when $P_p = 300$ mW, $P_{s,\mathrm{in}} = 1P_{\mathrm{in}}$, $\Delta\omega_G = 5$ GHz, and BR = 2 Gbps. The other parameters are: $\Gamma_B = 2\pi$ (30 MHz), $\Omega_B = 2\pi$ (9.6 GHz), $\alpha =$ 1 dB/km, $A = 15\,\mu\mathrm{m}^2$, $g_0 = 1.65\times10^{-11}$ m/W, and $L_{\mathrm{eff}} \simeq 1.6$ km, which are appropriate for the HNLF used in the experiment (see Fig. 1).

also seen that the smaller spectral components of the signal outside the 5 GHz bandwidth of the SBS gain profile are not amplified (the so-called filtering effect), which is the source of pattern-dependent distortion discussed above.

C. Detector Noise

Noise in the photodiode also degrades the SNR and IT. Shot-noise of the photocurrent gives rise to a mean-square current fluctuation equal to

$$\sigma_{\mathrm{sh}}^2 = 2q(RP_{s,\mathrm{out}} + i_d)\Delta\nu_e, \tag{11}$$

where i_d is the dark current and q is the electric charge. Johnson noise due to thermally excited carriers in the load resistor (resistance R_L) give fluctuations equal to

$$\sigma_{\mathrm{th}}^2 = \frac{4k_BT\Delta\nu_e}{R_L}. \tag{12}$$

The values of these parameters for our experiment are $R_L = 50\Omega$, $R = 0.5\,\mathrm{A/W}$, $i_d = 96.8\,\mathrm{nA}$, $\Delta\nu_e = 12\,\mathrm{GHz}$, $\Delta\nu_0 = 5\,\mathrm{GHz}$, and $T = 300\,\mathrm{K}$.

D. System Noise Analysis

We assume all noise sources introduced in Eqs. (7) and (9)–(12) are statistically independent so that we can add together all the noise terms to obtain the total variance of current fluctuation $\sigma_{\mathrm{tot}}^2 = \sigma_{\mathrm{sh}}^2 + \sigma_{\mathrm{th}}^2 + \sigma_{s-sp}^2 + \sigma_{sp-sp}^2 + \sigma_{\mathrm{aj}}^2$. The average current for the amplified signal in the photodiode is $I_{s,\mathrm{out}} = RP_{s,\mathrm{out}}$, giving a theoretically predicted SNR of $SNR_{\mathrm{th}} = I_{s,\mathrm{out}}/\sqrt{\sigma_{\mathrm{tot}}^2}$.

Figure 5 shows the theoretically predicted amplified signal and various noise sources as a function of P_p. At low SBS gain ($P_p \le 100\,\mathrm{mW}$), the detector shot-noise due to the dark current dominates, which will render the output signal indistinguishable. For $P_p > 100\,\mathrm{mW}$, the SBS gain amplifies the input signal over the detector noise floor, but other noise sources begin to grow. The noise contribution from amplitude jitter (σ_{aj}^2), which is due to the pattern dependence of the SBS slow-light effect, has a steeper slope than the other noise sources and becomes the dominant noise source for $P_p > 350\,\mathrm{mW}$. In light of the fact that the slow-light delay increases linearly with P_p, our results show that it is essential to minimize the pattern dependence in high-delay systems, which is enabled using a flattop gain profile, for example [20,26].

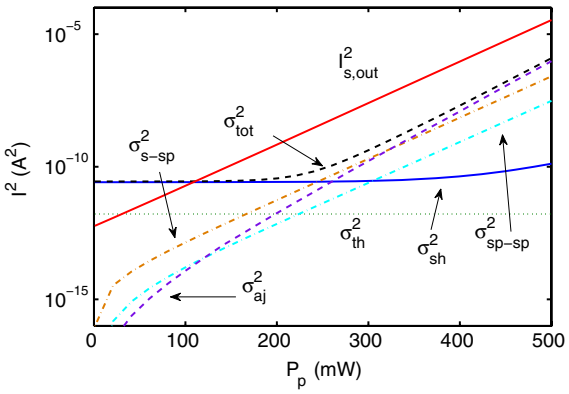

Fig. 5. (Color online) Theoretically predicted amplified signal and noise contributions from the various sources as a function of pump power for $P_{s,\mathrm{in}} = 1P_{\mathrm{in}}$, $\Delta\omega_G = 5\,\mathrm{GHz}$, and $\mathrm{BR} = 2\,\mathrm{Gbps}$. We account for the 7 dB attenuation due to the variable optical attenuator (VOA) used in the experimental setup.

5. Slow-light System Performance

We begin our discussion of the slow-light system performance by characterizing the shape of the gain profile and the scaling of gain and delay with P_p. To achieve a flattop gain profile, we follow the procedure described in [26]. Briefly, the AWG produces a fluctuating noisy voltage produced by uniformly distributed random function (clock rate of 400 MHz) that undergoes a nonlinear transformation. The transformation is adjusted in an iterative manner to obtain a gain profile that is as close to an ideal rectangular shape as possible.

Figure 6(a) shows the gain (defined as $G = \ln(P_{s,\mathrm{out}}/P_{s,\mathrm{in}})$) as a function of ω_s for $P_p = 70\,\mathrm{mW}$ and $P_{s,\mathrm{in}} \ll P_{\mathrm{in}}$ for a continuous-wave signal beam, where we see the gain profile has a flattop of width $\Delta\omega_G/2\pi = 5\,\mathrm{GHz}$ and reasonably sharp edges. As discussed in [26], the departure of this profile from the ideal rectangular shape has a minimal impact on the slow-light delay and distortion. Figure 6(b) shows that the gain at the center of the profile scales linearly with P_p. A maximum exponential gain of ~9 at $P_p = 500\,\mathrm{mW}$ ensures that we only experience mild pump depletion when $P_{s,\mathrm{in}} = 1P_{\mathrm{in}}$, as discussed below. Correspondingly, the slow-light fractional delay (FD) also scales linear with P_p for $P_{s,\mathrm{in}} \ll P_{\mathrm{in}}$, as seen in Fig. 6(c). Here, we inject a *single* super-Gaussian pulse with a FWHM pulse width of $T_p = 200\,\mathrm{ps}$ and measure the delay ΔT_d between the peak of the output pulse with the pump-beam turned on and with it turned off. The FD is then defined as $\Delta T_d/T_p$. Measuring

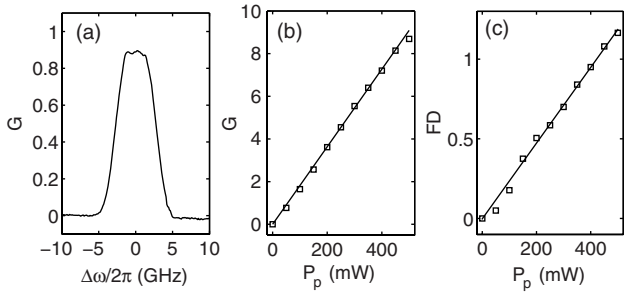

Fig. 6. (a) Flattop SBS gain spectrum with a width (FWHM) equal to 5 GHz for $P_p = 70\,\mathrm{mW}$. (b) Gain and (c) pulse-peak-to-pulse-peak fractional slow delay experienced by a single super-Gaussian pulse of duration (FWHM) $T_p = 200\,\mathrm{ps}$ as a function of the pump power. The straight lines in (b) and (c) are a guide to the eye and consistent with the linear scaling expected for the slow-light system.

the delay of the pulse peak is one method used frequently by the slow-light community. We fix $\Delta\omega_G/2\pi = 5$ GHz for all of the numerical and experimental studies described below.

To investigate the pattern dependence and the affects of noise in our slow-light system, we propagate all 8 bit sequences through the channel with BR = 2 Gbps and $P_{s,\mathrm{in}} = 1P_{\mathrm{in}}$. Eye diagrams are created by overlaying the pulse sequences timed with respect to the trigger produced by the pattern generator. Figure 7 shows the experimentally measured and theoretically predicted eye diagrams for a range of values of P_p. The top panels show the eye diagram of the undelayed (denoted as the input) sequence obtained by setting $P_p = 0$, removing the attenuator in front of the detector, and increasing $P_{s,\mathrm{in}}$ so that we are just below the detector saturation. We find EO = 0.61 for the experimentally measured input sequences, which takes on a finite value because of the residual detector noise and slight distortion of the pulses produced by our pattern generator. For the measurements described next, we return the detection system and the signal power to their nominal operating conditions.

For low pump powers ($P_p = 100$ mW), the SBS gain is so low that the pulses do not appear above the noise floor of our detection system and the eye diagram is completely closed. For increasing P_p, the SBS gain is sufficient to pull the pulses out of the noise and the EO increases. At $P_p = 500$ mW, ASE and pattern dependence induced by the slow-light channel, enhanced by slight saturation of the SBS gain, cause a slight decrease in the EO. In this case, we find FD ~0.83, SNR ~5.52, and EO ~0.52. We also find good qualitative agreement between observations and predictions.

To make a quantitative comparison between experiment and theory and to explore the affects of changing $P_{s,\mathrm{in}}$, we propagate all 8 bit data sequences through the slow-light channel 10 times for each value of $P_{s,\mathrm{in}}$. The fractional ID (FID) and IT of the experimental time series is determined using the procedure described at the end of Section 3. Figure 8 summarizes our findings for $P_{s,\mathrm{in}} = (0.5, 1, 2)P_{\mathrm{in}}$. From Fig. 8(a), we see that the FID scales linearly over the entire range when $P_{s,\mathrm{in}} = 0.5P_{\mathrm{in}}$. For $P_{s,\mathrm{in}} > 0.5P_{\mathrm{in}}$, we observe saturation of the FID at the highest pump powers, which is due to pump depletion occurring at high SBS gain. This saturation effect is not accounted for in our model; in particular, Eq. (4) assumes that there is no pump depletion.

The SNR [Fig. 8(c)] initially grows rapidly with increasing P_p and then decreases due to the fact that the ASE noise, slow-light pattern dependence, and gain saturation increases faster than the signal amplification. The largest maximum value of the SNR occurs for the largest value of $P_{s,\mathrm{in}}$ because the higher input signal power is more able to overcome the detection system noise. At $P_p = 500$ mW, the SNR is similar for all input signal powers due to saturation of the SBS gain. We find a trade-off between SNR and FID because the largest delay is achieved for the smallest input power at the cost of smaller SNR. Note that similar behavior of the SNR for a Brillouin amplifier without pump-beam spectral broadening was observed in [43,44].

The EO and IT both follow similar trends. In particular, the initial onset in growth of the EO or IT occurs at a lower value of P_p for the larger value of $P_{s,\mathrm{in}}$. At the higher pump powers, they decrease for the same reason for the decrease in the SNR. The inset to Fig. 8(d) shows that the IT exceeds 0.9 over a wide range of P_p (and hence slow-light delays). Interestingly, the widest range of P_p over which IT > 0.9 occurs for the highest value of $P_{s,\mathrm{in}}$ due to a balance between having enough signal power to overcome detector noise and avoiding SBS gain saturation.

We now investigate the affects of changing the data rate. Recall from Fig. 4 that the signal spectrum occupies a width of approximately 4 GHz for a RZ modulation format with BR = 2 Gbps. Here, we characterize the affects of changing BR so that it fully occupies the bandwidth of the SBS resonance (BR = 2.5 Gbps) and somewhat exceeds it (BR = 2.86 Gbps). Figure 9

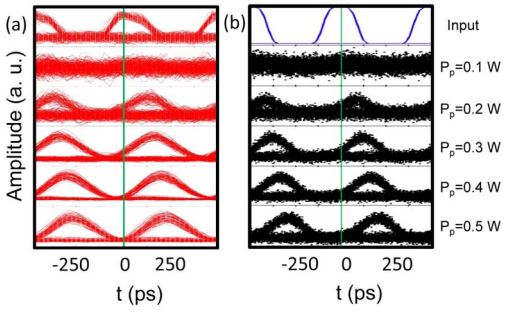

Fig. 7. (Color online) Input and output eye diagrams for several different pump powers, $P_{s,\mathrm{in}} = 1P_{\mathrm{in}}$ and BR = 2 Gbps. (a) Experimental results measured by an oscilloscope and (b) numerical simulations.

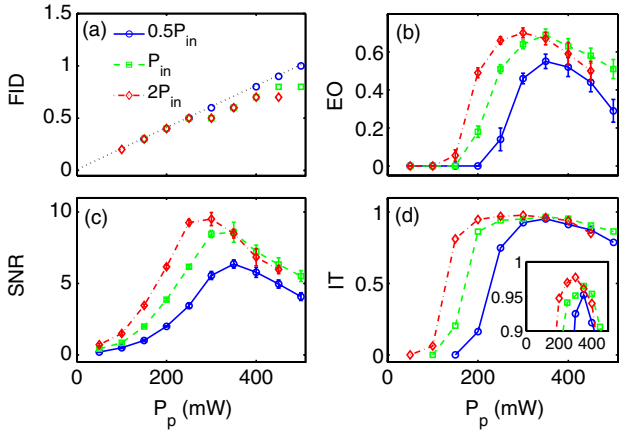

Fig. 8. (Color online) Delay and data fidelity metrics as a function of input signal power for BR = 2 Gbps. (a) Fractional information delays are denoted by the symbols. The dashed straight line is a guide to the eye and consistent with the linear scaling expected for a slow-light system. (b) Eye opening, (c) SNR, and (d) IT as a function of P_p.

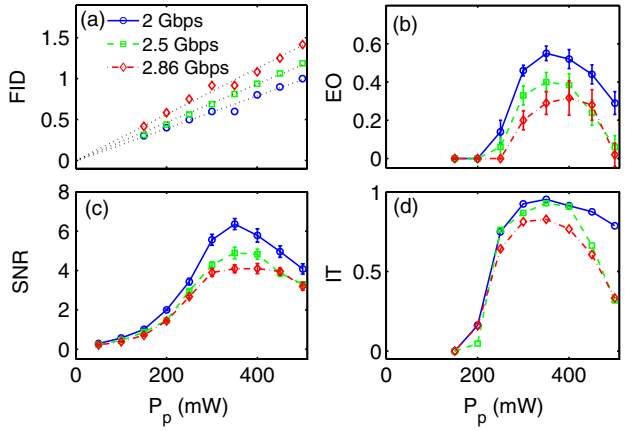

Fig. 9. (Color online) Delay and data fidelity metrics as a function of data rate for $P_{s,\mathrm{in}} = 0.5P_{\mathrm{in}}$. (a) Fractional information delays are denoted by the symbols. The dashed straight lines are a guide to the eye. (b) Eye opening, (c) SNR, and (d) IT as a function of P_p.

summarizes our findings, where we see that there is a notable trade-off between data rate and signal fidelity. In particular, we see that higher BR give a larger FID [Fig. 9(a)] because the data-pulse width is smaller, yet the slow-light gain and delay are comparable. However, the signal fidelity decreases for increasing BR as quantified by all three metrics (EO, SNR, and IT, Figs. 9(b)–9(d), respectively). The loss of signal integrity is due to the strong signal filtering effect of the SBS amplification process. For all data rates, the IT grows quickly beyond $P_p = 200\,\mathrm{mW}$, but decreases most rapidly for the highest BR as P_p increases. Clearly, the broadest range of high IT occurs when the signal spectrum fits well within the SBS gain spectrum, but at the cost of substantially lowered FID. The general trends for delay and fidelity based on the use of all three metrics agree well and strongly depend on the input signal BR.

Finally, we compare the performance of using an optimal flattop gain profile with a Gaussian-shaped profile. The Gaussian-shaped profile is obtained by driving the signal laser with a random noise voltage without the use of a nonlinear transformation [15,26],

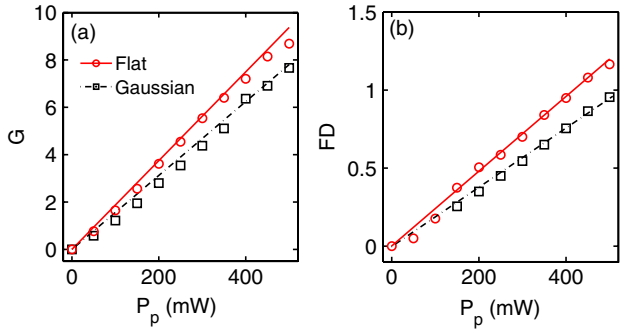

Fig. 10. (Color online) (a) Gain and (b) fractional delay for the optimal flattop and Gaussian gain profiles of width (FWHM) of 5 GHz. The measurements are made when propagating a single weak super-Gaussian pulse with $T_p = 200\,\mathrm{ps}$ through the slow-light medium. The solid and dashed straight lines are guides to the eye.

where the noise amplitude is adjusted to give the same width (FWHM) for both profiles. Based on previous studies [19,20,26], we expect that the flattop profile will give larger FD and higher data fidelity for the same P_p, which is highly desirable in a slow-light system operating in a limited-resource environment where the pump power and maximum SBS gain are constrained. Figure 10 compares the gain and FD for the case when a single super-Gaussian pulse with $\Delta T_p = 200\,\mathrm{ps}$ propagates through the slow-light systems. The optimal flattop profile clearly outperforms the Gaussian gain in terms of delay over all P_p, enabling FD $\sim$1.2 ($\Delta T_d = 240\,\mathrm{ps}$) at $P_p = 500\,\mathrm{mW}$, which is $\sim$1.23 times the maximum delay for the Gaussian-shaped profile.

To determine the data fidelity, we again pass all 8 bit time sequences through the slow-light system for each profile as a function of P_p for BR = 2.5 Gbps and $P_{s,\mathrm{in}} = 1P_{\mathrm{in}}$. These results are summarized in Fig. 11. It is seen that the FID for the optimal flattop profile increases linearly with P_p with a larger slope that the case of the Gaussian profile, consistent with Fig. 10(b). Furthermore, all data fidelity metrics are the same or somewhat larger for the optimal profile in comparison to the Gaussian for a given P_p. In greater detail, we find that the optimal profile gives a 36% larger ID compared to the Gaussian profile: The optimal (Gaussian) profile produces a FID of 0.94 (0.69) and an IT of 0.86 (0.86) for $P_p = 450\,\mathrm{mW}$. Thus, the optimal profile better utilizes the available pump-beam power, which is often a valuable resource in a system design. Especially noteworthy is the observation that the IT for the flattop profile saturates more slowly than the Gaussian for large P_p, increasing the range of delays over which high-fidelity data transmission is possible. Note that we also measured the fractional EO delay, which agrees closely with the FID and therefore is not shown on the figures.

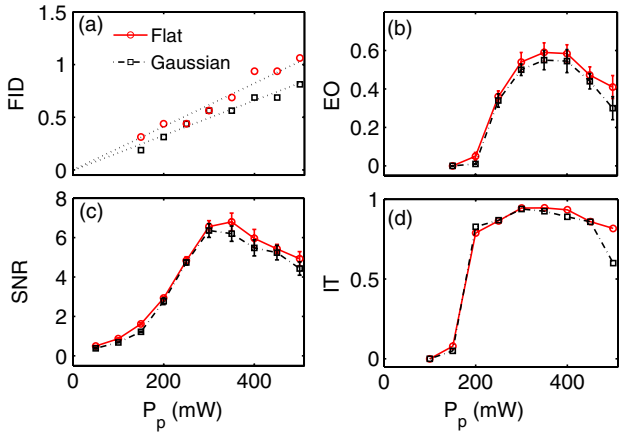

Fig. 11. (Color online) Delay and data fidelity metrics for the flattop and Gaussian gain profiles for BR = 2.5 Gbps and $P_{s,\mathrm{in}} = 1P_{\mathrm{in}}$. (a) Fractional information delay is denoted by the symbols. The dashed straight lines are a guide to the eye. (b) Eye opening, (c) SNR, and (d) IT as a function of P_p.

6. Discussion and Conclusions

In conclusion, we use a recently developed information-theoretic framework [30] for quantifying the delay and signal fidelity of a slow-light system based on SBS in a room-temperature single-mode fiber pumped by a spectrally-broadened laser. We show that the IT increases with increasing SNR, as expected from basic information theory [31]. The IT formalism relies on comparing the *entire input and output pulse sequences* rather than measuring them only at a specific instant of time as is done in computing the SNR and EO metrics. The IT is large when the output signal pattern is distinct (*i.e.*, an open eye diagram) and reaches its maximum when the output signal has the largest data fidelity, consistent with other popular measures of data fidelity, such as the SNR and EO. We emphasize that the IT grows rapidly with increasing SNR for small values of the SNR. Because of these characteristics, we claim that the IT metric gives a more useful system-wide measure of data fidelity.

Our investigation has highlighted several trade-offs in slow-light delay and data fidelity. For example, lower input signal powers are appropriate for high pump powers (and hence large delays) because the lower powers delay the onset of gain saturation. On the other hand, higher input signal powers are appropriate for smaller delays so that the output signal overcomes the detector noise. As another example, higher data rates for a fixed bandwidth of the SBS gain profile gives rise to larger fractional slow-light delay, but comes at the cost of lower data fidelity. Finally, the use of a flattop gain profile is superior to a Gaussian profile in that larger slow-light delay can be obtained for lower pump powers. These results demonstrate that IT- and ID-based analyses are important components of the tools for designing slow-light systems and understanding limits and trade-offs. While aspects of our study are specific to our choice of a slow-light medium and system parameter choices, we believe that the factors we identify will be important in other systems.

We gratefully acknowledge the financial support of the Defense Advanced Research Projects Agency (DARPA) Defense Sciences Office Slow-Light Program.

References

1. R. W. Boyd and D. J. Gauthier, "Controlling the velocity of light pulses," Science **326**, 1074–1077 (2009).
2. R. S. Tucker, P. C. Ku, and C. J. Chang-Hasnain, "Slow-light optical buffers: capabilities and fundamental limitations," J. Lightwave Technol. **23**, 4046–4066 (2005).
3. Z. Bo, L. Yan, J. Yang, I. Fazal, and A. Willner, "A single slow-light element for independent delay control and synchronization on multiple Gb/s data channels," IEEE Photon. Technol. Lett. **19**, 1081–1083 (2007).
4. Z. Shi, R. W. Boyd, R. M. Camacho, P. K. Vudyasetu, and J. C. Howell, "Slow-light Fourier transform interferometer," Phys. Rev. Lett. **99**, 240801 (2007).
5. Z. Shi and R. W. Boyd, "Slow-light interferometry: practical limitations to spectroscopic performance," J. Opt. Soc. Am. B **25**, C136–C143 (2008).
6. R. Zhang, Y. Zhu, J. Wang, and D. J. Gauthier, "Slow light with a swept-frequency source," Opt. Express **18**, 27263–27269 (2010).
7. A. Schweinsberg, Z. Shi, J. E. Vornehm, and R. W. Boyd, "Demonstration of a slow-light laser radar," Opt. Express **19**, 15760–15769 (2011).
8. M. Gonzalez-Herraez, K. Song, and L. Thévenaz, "Optically controlled slow and fast light in optical fibers using stimulated Brillouin scattering," Appl. Phys. Lett. **87**, 081113 (2005).
9. Y. Okawachi, M. S. Bigelow, J. E. Sharping, Z. Zhu, A. Schweinsberg, D. J. Gauthier, R. W. Boyd, and A. L. Gaeta, "Tunable all-optical delays via Brillouin slow light in an optical fiber," Phys. Rev. Lett. **94**, 153902 (2005).
10. Z. Zhu, D. J. Gauthier, Y. Okawachi, J. E. Sharping, A. L. Gaeta, R. W. Boyd, and A. E. Willner, "Numerical study of all-optical slow-light delays via stimulated Brillouin scattering in an optical fiber," J. Opt. Soc. Am. B **22**, 2378–2384 (2005).
11. M. D. Stenner, M. A. Neifeld, Z. Zhu, A. M. C. Dawes, and D. J. Gauthier, "Distortion management in slow-light pulse delay," Opt. Express **13**, 9995–10002 (2005).
12. A. Minardo, R. Bernini, and L. Zeni, "Low distortion Brillouin slow light in optical fibers using AM modulation," Opt. Express **14**, 5866–5876 (2006).
13. A. Zadok, A. Eyal, and M. Tur, "Extended delay of broadband signals in stimulated Brillouin scattering slow light using synthesized pump chirp," Opt. Express **14**, 8498–8505 (2006).
14. T. Schneider, M. Junker, and K.-U. Lauterbach, "Potential ultra wide slow-light bandwidth enhancement," Opt. Express **14**, 11082–11087 (2006).
15. Z. Zhu, A. M. C. Dawes, D. J. Gauthier, L. Zhang, and A. E. Willner, "Broadband SBS Slow Light in an Optical Fiber," J. Lightwave Technol. **25**, 201–206 (2007).
16. Z. Shi, R. Pant, Z. Zhu, M. D. Stenner, M. A. Neifeld, D. J. Gauthier, and R. W. Boyd, "Design of a tunable time-delay element using multiple gain lines for large fractional delay with high data fidelity," Opt. Lett. **32**, 1986–1988 (2007).
17. L. Yi, Y. Jaouen, W. Hu, Y. Su, and S. Bigo, "Improved slow-light performance of 10 Gb/s NRZ, PSBT and DPSK signals in fiber broadband SBS," Opt. Express **15**, 16972–16979 (2007).
18. Z. Lu, Y. Dong, and Q. Li, "Slow light in multi-line Brillouin gain spectrum," Opt. Express **15**, 1871–1877 (2007).
19. R. Pant, M. D. Stenner, M. A. Neifeld, and D. J. Gauthier, "Optimal pump profile designs for broadband SBS slow-light systems," Opt. Express **16**, 2764–2777 (2008).
20. E. Cabrera-Granado, O. G. Calderon, S. Melle, and D. J. Gauthier, "Observation of large 10 Gb/s SBS slow light delay with low distortion using an optimized gain profile," Opt. Express **16**, 16032–16042 (2008).
21. T. Sakamoto, T. Yamamoto, K. Shiraki, and T. Kurashima, "Low distortion slow light in flat Brillouin gain spectrum by using optical frequency comb," Opt. Express **16**, 8026–8032 (2008).
22. Y. Dong, Z. Lu, Q. Li, and Y. Liu, "Broadband Brillouin slow light based on multifrequency phase modulation in optical fibers," J. Opt. Soc. Am. B **25**, C109–C115 (2008).
23. M. Lee, R. Pant, and M. A. Neifeld, "Improved delay performance of broadband stimulated Brillouin Scattering (SBS) slow-light system using fiber Bragg gratings," Appl. Opt. **47**, 6404–6415 (2008).
24. Z. Zhang, X. Zhou, R. Liang, and S. Shi, "Influence of third-order dispersion on delay performance in broadband Brillouin slow light," J. Opt. Soc. Am. B **26**, 2211–2217 (2009).
25. S. Chin, M. Gonzalez-Herraez, and L. Thévenaz, "Complete compensation of pulse broadening in an amplifier-based slow

light system using a nonlinear regeneration element," Opt. Express **17**, 21910–21917 (2009).
26. Y. Zhu, M. Lee, M. A. Neifeld, and D. J. Gauthier, "High-fidelity broadband stimulated-Brillouin-scattering-based slow light using fast noise modulation," Opt. Express **19**, 687–697 (2011).
27. R. W. Boyd, D. J. Gauthier, A. L. Gaeta, and A. E. Willner, "Erratum: Maximum time delay achievable on propagation through a slow-light medium," Phys. Rev. A **72**, 059903 (2005).
28. J. B. Khurgin, "Performance limits of delay lines based on optical amplifiers," Opt. Lett. **31**, 948–950 (2006).
29. D. A. B. Miller, "Fundamental limit to linear one-dimensional slow light structures," Phys. Rev. Lett. **99**, 203903 (2007).
30. M. A. Neifeld and M. Lee, "Information theoretic framework for the analysis of a slow-light delay device," J. Opt. Soc. Am. B **25**, C31–C38 (2008).
31. C. E. Shannon, "A mathematical theory of communications," Bell Syst. Tech. J. **27**, 379–423 (1948).
32. B. Zhang, L. Yan, I. Fazal, L. Zhang, A. E. Willner, Z. Zhu, and D. J. Gauthier, "Slow light on Gbit/s differential-phase-shift-keying signals," Opt. Express **15**, 1878–1883 (2007).
33. G. P. Agrawal, *Fiber-Optic Communication Systems*, 3rd ed. (Wiley, 2002).
34. Z. Zuqing, M. Funabashi, P. Zhong, X. Bo, L. Paraschis, and S. J. B. Yoo, "Jitter and amplitude noise accumulations in cascaded all-optical regenerators," J. Lightwave Technol. **26**, 1640–1652 (2008).
35. J. D. Fast, *Entropy. The Significance of the Concept of Entropy and Its Applications in the Science and Technology* (McGraw-Hill, 1962).
36. S. Le Floch and P. Cambon, "Theoretical evaluation of the Brillouin threshold and the steady-state Brillouin equations in standard single-mode optical fibers," J. Opt. Soc. Am. A **20**, 1132–1137 (2003).
37. Y. Zhu, E. Cabrera-Granado, O. G. Calderon, S. Melle, Y. Okawachi, A. L. Gaeta, and D. J. Gauthier, "Competition between the Modulation Instability and Stimulated Brillouin Scattering in a Broadband Slow Light Device," J. Opt. **12**, 104019 (2010).
38. R. Holzlohner, H. N. Ereifej, V. S. Grigoryan, G. M. Carter, and C. R. Menyuk, "Experimental and theoretical characterization of a 40 Gb/s long-haul single-channel transmission system," J. Lightwave Technol. **20**, 1124–1131 (2002).
39. S. Norimatsu and M. Maruoka, "Accurate *Q*-factor estimation of optically amplified systems in the presence of waveform distortions," J. Lightwave Technol. **20**, 19–27 (2002).
40. R. W. Boyd, K. Rzaewski, and P. Narum, "Noise initiation of stimulated Brillouin scattering," Phys. Rev. A **42**, 5514–5521 (1990).
41. S. Sternklar, Y. Glick, and S. Jackel, "Noise limitations of Brillouin two-beam coupling: theory and experiment," J. Opt. Soc. Am. B **9**, 391–394 (1992).
42. N. A. Olsson, "Lightwave systems with optical amplifiers," J. Lightwave Technol. **7**, 1071–1082 (1989).
43. A. Ghosh, D. Venkitesh, and R. Vijaya, "Study of Brillouin amplifier characteristics toward optimized conditions for slow light generation," Appl. Opt. **48**, G48–G52 (2009).
44. F. Ravet, X. Bao, J. Snoddy, Y. Li, and L. Chen, "Characterization of Brillouin fiber generator and amplifier for optimized working condition of distributed sensors," Opt. Fiber Technol. **15**, 304–309 (2009).